J. of Thermal Science Vol.10, No.2

Numerical Prediction of Fluid Flow and Heat Transfer in a Wavy Pipe

Shohel Mahmud **A.K.M. Sadrul Islam** **Prodip Kumar Das**
Department of Mechanical Engineering, Bangladesh University of Engineering & Technology, BUET, Dhaka-1000, Bangladesh

Hydrodynamic and thermal characteristics in a pipe with sinusoidal wavy surface for steady laminar flow are investigated numerically in the present study. The integral forms of governing equations are discretized using control volume based Finite Volume method with collocated variable arrangement. SIMPLE algorithm is used and TDMA solver is applied for solution of system of equations. A pipe of length equal to 4λ is considered. Effect of surface waviness, determined by wavelength-amplitude ratio λ/a ($=L^*$), on flow and thermal field is presented. The simulation work has been carried out for L^*=11.0 -30.0 for a Reynolds number range 50 to 2000. Results are presented in the form of streamfunction, isothermal lines, velocity and vorticity profiles, change of mean friction factor, variation in skin friction, local and average Nusselt number with Reynolds number, wave number (n) and L^*. For a particular geometry, length of circulation zone increases with Reynolds number and approaches a limiting value for higher Reynolds number. Wall shear stress in the bulge part of the channel shows smaller values that affect largely the rate of heat transfer and Nusselt number shows minimum values in this region. This circulation zone drastically increases with the increase of surface waviness showing high mean friction factor per wavelength. Mean friction factor inversely varies with Reynolds number. A correlation is proposed for calculating friction factor in the form $f=C/(Re)^m$, where 'C' and 'm' represents two polynomials of degree 4 and 2 respectively and are function of L^*. Higher waviness of the surface shows the higher heat transfer rate than lower waviness. Heat transfer rate falls almost exponentially along the axial direction with the increase of wave number.

Keywords: Nusselt number, separation bubble, surface waviness, wall vorticity

Introduction

A pipe with periodically converging-diverging cross-section is one of the several devices employed for enhancing the heat and mass transfer efficiency. The fluid flow, in the flow passages with a periodically varying cross-section, attains a fully developed regime that differs fundamentally from that for a conventional constant-area flow channel. In the periodically varying cross-sections, the fully developed velocity field repeats itself at corresponding axial locations in successive cycles. The change of flow pattern with changes in duct dimensions is a special feature of the complex corrugated-duct geometry that is not encountered in conventional ducts such as circular and annular pipes and rectangular ducts. Flow through wavy or corrugated channel serves as a simple example of separated flow, in which the complex interactions of separated vortices, free shear layers, driving wall-bounded shear flows can be examined in some details. These types of channel widely used for heat transfer augmentation in recent years. Geometrical complexity of such channel or ducts affects largely the flow pattern. Their fabrication depends on many parameters like amplitude, wavelength, phase angle, inter-wall spacing, corrugation angle, sharpness or roundness of successive peaks and valleys of the walls etc. and each of the parameter significantly affects the hydrodynamic behavior of fluid flow through this channel. These configurations are not idealities and its effect on flow phenomenon motivates many researchers to perform experimental or analytical work on this topic.

Saidi et. al.[1] studied laminar flow past a sinusoidal cavity. They presented how the increase of flow velocity

Received 2000

Nomenclature

a	amplitude	v	radial component of velocity
C	correlation constant	U_0	free stream velocity
C_f	skin friction coefficient, $(2\tau_w/\rho U_m^2)$	U_m	mean velocity
D	Diameter of the wavy channel	x	axial distance
f	friction factor per wave length	X	normalized axial distance, (x/λ)
L	length of the pipe		**Greek symbols**
L^*	geometric parameter, (λ/a)	ρ	density of fluid
m	exponent of the correlation	μ	viscosity
n	wave number	ψ	normalized stream function
Nu_X	local Nusselt number	θ	dimensionless temperature
Nu_{av}	average Nusselt number	τ	shear stress, $(\mu du/dr)$
r	radial distance	ξ	vorticity, $(0.5\ Re\ C_f D_{max}/D_{av})$
R	normalized radial distance, (r/λ)	λ	wavelength
Re	Reynolds number, $(\rho U_m D_{av}/\mu)$	Γ	diffusion coefficient
S	surface area		**Subscript**
T	field temperature	w	at wall
T_W	wall temperature	i,j	Cartesian notation of x & y direction
T_α	fluid temperature	av	average value
u	axial component of velocity	max	maximum value
		min	minimum value

gives birth of vortex inside cavity and affects hydrodynamic and thermal performance. Wang and Vanka[2] reported higher values of friction factor for wavy channel compared to the parallel plate channel of same interwall spacing. Yang et. al.[3] carried out computation using low Reynolds number turbulent model for three different inner wall spacing for $100<Re<2500$ in a corrugated wall channel and reported transitional Reynolds number is lower than the value for the parallel plate duct and it decreases with increasing corrugation angle. Nishimura et al.[4] investigated flow characteristics such as flow pattern, pressure drop and wall shear stress in a channel with symmetric sinusoidal wavy wall. This study reported that for Reynolds number greater than 700, turbulent flow occurs, owing to the onset of unsteady vortex motion and friction factor is inversely proportional to Reynolds number at the laminar range. Russ and Beer[5,9] calculated mean friction coefficient wavelength of axisymmetric pipe for three different amplitudes and reported frictional loss increases with the increase of amplitude at same Reynolds number. Sparrow and Hossfeld[7] performed experimental study to determine the heat transfer, pressure drop, and flow field responses to the rounding of the peaks of a corrugated wall duct at a Reynolds number range 2000 to 33000. They reported that due to rounding off, friction factor decreases corresponding to a given Reynolds number even more than did the Nusselt number. Other references[8~11] have reported the flow characteristics and heat transfer inside wavy channel. This paper mainly discusses the effect of surface waviness on flow pattern, shear stress and pressure drop characteristics and heat transfer inside a pipe with wavy surface.

Problem Formulation

Fig.1 shows the geometry considered in the present investigation. The governing equations for steady, incompressible, laminar flow in the integral form[12] is:

$$\int_S \rho\, \mathbf{v}.\mathbf{n}\, ds = 0 \tag{1}$$

$$\int_S \rho u_i\, \mathbf{v}.\mathbf{n}\, ds = \int_S \mu \mathrm{grad} u_i.\mathbf{n}\, ds - \int_S p\mathbf{i}_i.\mathbf{n}\, ds + \int_V \rho b_i dv \tag{2}$$

$$\int_S \rho u_j\, \mathbf{v}.\mathbf{n}\, ds = \int_S \mu \mathrm{grad} u_j.\mathbf{n}\, ds - \int_S p\mathbf{i}_j.\mathbf{n}\, ds + \int_V \rho b_j dv \tag{3}$$

$$\int_S \rho T\, \mathbf{v}.\mathbf{n}\, ds = \int_S k \mathrm{grad} T.\mathbf{n}\, ds \tag{4}$$

Equations (1) - (4) can be written in a generalized form:

$$\int_S \rho\phi\, \mathbf{v}.\mathbf{n}\, dS = \int_S \Gamma\, \mathrm{grad}\phi.\mathbf{n}\, dS + \int_V q_\phi dV \tag{5}$$

Numerical solution

The integral form of governing equations is discretized using control volume based Finite Volume method. The solution domain is first subdivided into a finite number of contiguous control volumes (CVs), and the conservation equations are applied to each CV. At the centroid of each CV lies a computational node at which the variable values are to be calculated. The computational node at which all unknowns are stored in one dimensional arrays and sorted level-wise, starting

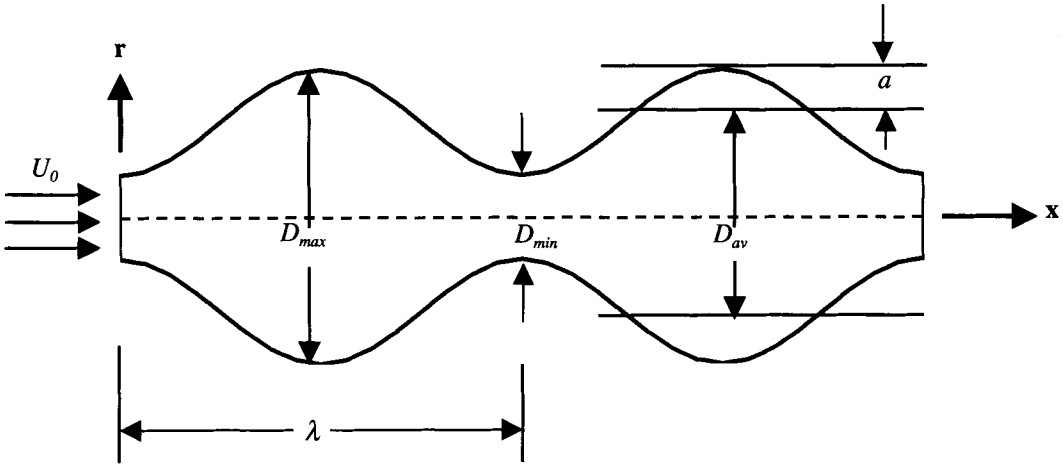

Fig.1 Schematic diagram of a portion of geometry under consideration (Total length is 4λ)

with level 1 (coarse grid) to level 3 (fine grid). Collocated arrangement is used for variables, i.e. all variables are calculated at the same CV center. Both surface and volume integrals in the conservation equations (1) (5) are approximated here using midpoint rule, i.e. the value of the integrand at the center of cell face or CV is multiplied by the face area or CV volume. Mass flux through any face of the CV is calculated using the relation:

$$\dot{m} = \int_S \rho \, \boldsymbol{v}.\boldsymbol{n} \, dS \approx (\rho \, \boldsymbol{v}.\boldsymbol{n})S \qquad (6)$$

The convective flux of any transported quantity is calculated by assuming that the mass flux is known which, with midpoint rule approximation[12,13] leads to:

$$F_C = \int_S \rho \phi \boldsymbol{v}.\boldsymbol{n} \, dS \approx \dot{m}\phi \qquad (7)$$

The midpoint rule applied to the diffusive flux gives:

$$F_d = \int_S \Gamma \, grad \, \phi . \boldsymbol{n} \, dS \approx (\Gamma \, grad \, \phi . \boldsymbol{n})S \qquad (8)$$

The gradient of φ at the cell face center can be expressed in the form:

$$grad \, \phi = \frac{\partial \phi}{\partial x}\boldsymbol{i} + \frac{\partial \phi}{\partial y}\boldsymbol{j} \qquad (9)$$

In general the diffusive fluxes are calculated using the elation:

$$F_d = \Gamma \sum_i \left(\frac{\partial \phi}{\partial x_i}\right) S^i \qquad (10)$$

The final discretized form of governing equations is solved iteratively using TDMA solver. Iteration is continued until difference between two consecutive field values of variables is less than or equal to 10^{-5}. For further stabilization of numerical algorithm, under relaxation factors of 0.1-0.7 are used.

Results and Discussions

In the present investigation, a pipe of length 4λ is considered. For simplicity, only two cycles are shown in Fig.1. The radius of the pipe follows a sine curve and is given by:

$$r = a\left[1\text{-}Sin\frac{\pi}{2}\left(1+4x/\lambda\right)\right] + D_{min}/2 \qquad (11)$$

Computations were carried out for three grid sizes (140 × 16, 280 × 32, 560 × 64). Fig.2 shows the axial velocity profiles for these three grid sizes. Coarse grid shows some deviation from medium coarse and fine grid. Fine-grid (560×64) results are presented in this paper. Fig.3 shows the comparison of present prediction with experimental data of friction factor of Russ and Beer [6]. Both experimental and numerical results show good agreement.

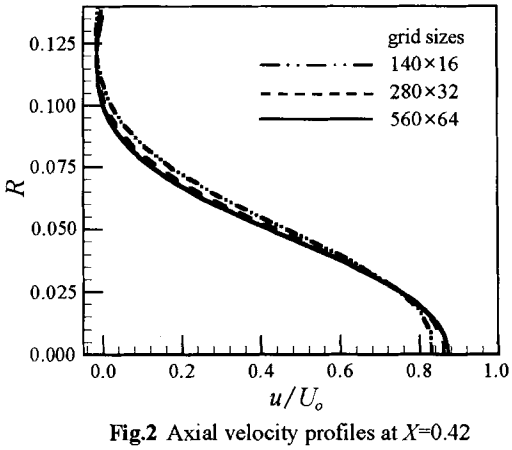

Fig.2 Axial velocity profiles at X=0.42 for L^*=19.0, Re=600

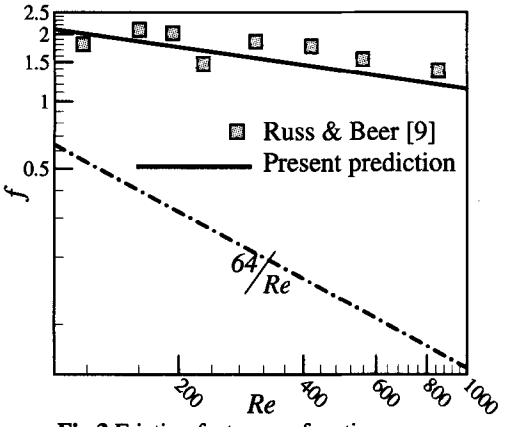

Fig.3 Friction factor as a function of Re for L^*=19.0

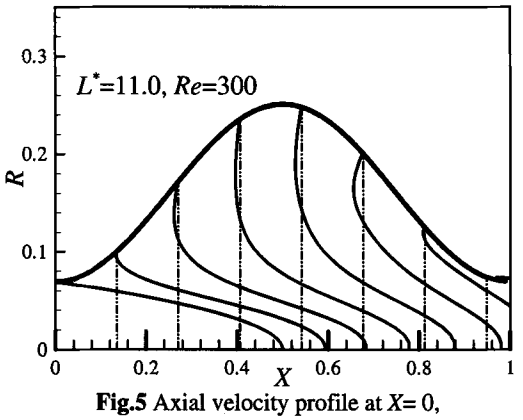

Fig.5 Axial velocity profile at X= 0, $\lambda/7$, $2\lambda/7$, $3\lambda/7$, $4\lambda/7$, $5\lambda/7$, $6\lambda/7$

Flow pattern

Flow fields are expressed by streamlines and axial velocity profiles. Fig.4 shows the streamlines for L^*=11.0 at Re=300. Flow separates as fluid moves downstream into the diverging portion and reattaches on the converging portion. Core of the separation bubble shifts downstream with the increase of Reynolds number. Streamlines for other geometry shows the similar pattern except the size of the separation bubble. Separation region is smaller at the same Reynolds number for lower wavy (higher L^*) surface. Fig.5 shows the axial velocity profiles for Re=300. Profile in the narrowest cross-section shows larger wall velocity gradient compared to the parabolic profile of the flow through a straight pipe. Before maximum cross-section, velocity gradient near the wall becomes zero with positive pressure gradient causing separation. Separated region is characterized by separation bubble in the bulge part of the pipe shown in Fig.4 and Fig.5. In the converging part, the axial pressure gradient changes its sign again (positive to negative) causing reattachment. Somewhere near the reattachment point, negative axial velocity shows its

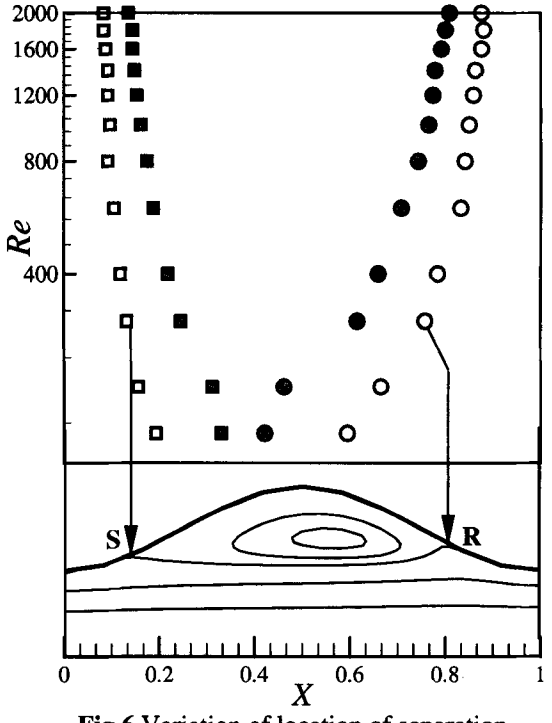

Fig.6 Variation of location of separation and reattachment point with Re for L^*=11.0 (open symbol) and L^*=23.0 (filled symbol)

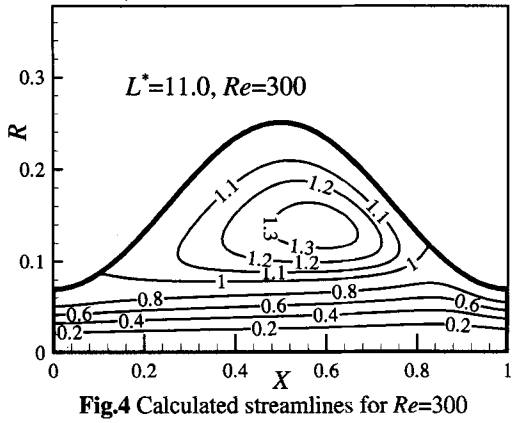

Fig.4 Calculated streamlines for Re=300

maximum gradient. Fig.6 explains how separation and reattachment points changes with Reynolds number for L^*=11.0 (high waviness) and L^*=23.0 (low waviness).

Wall shear stress

The calculated wall vorticity profiles are shown in Fig.7 for Re=2000 at fourth cycle. For low wall waviness (e.g. L^*=30.0), wall vorticity profile is symmetrical about the maximum cross-section and positive everywhere. As the surface waviness increases, vorticity near the

maximum cross-section becomes negative. Magnitude of negative vorticity increases with the increase of waviness of the wall. Vorticity at the separation and reattachment point is zero due to zero velocity gradient. The minimum point (negative maximum) of vorticity occurs near the reattachment point due to maximum negative velocity gradient and shifts downstream side with higher magnitude (negative) with the increase of wall waviness.

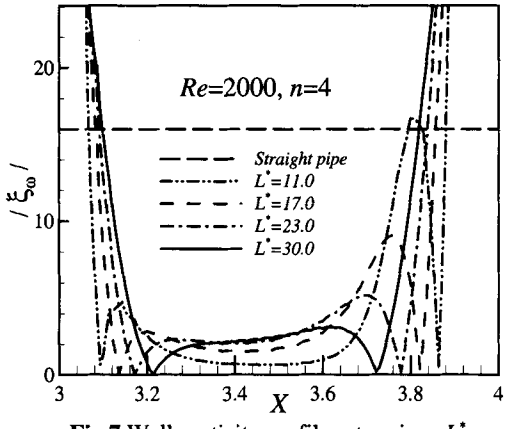

Fig.7 Wall vorticity profiles at various L^*

Pressure drop

Pressure drop along the wavy pipe is calculated in terms of average friction factor per cycle. Fig.8 shows the variation of friction factor with Reynolds number at different L*. Larger surface waviness shows higher frictional loss at the same Reynolds number.

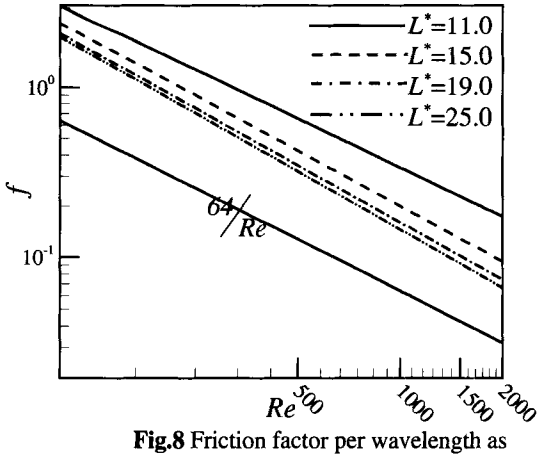

Fig.8 Friction factor per wavelength as a function of Reynolds number

The linear variation of friction factor with Reynolds number in logarithmic plot enables to make a correlation between friction factor (f), Reynolds number (Re) and geometric parameter (L*). The proposed correlation is in the form:

$$f = C/Re^m \tag{12}$$

Correlation constant (C) and exponent (m) are calculated from the intersection and slope of the curves of Fig.8 respectively at different geometric parameter L^*. The values of 'C' and 'm' are then plotted against L^* shown in Fig.9. The equation of best-fit curves of Fig.9 follows two polynomials of order 4 and 2 respectively. These are:

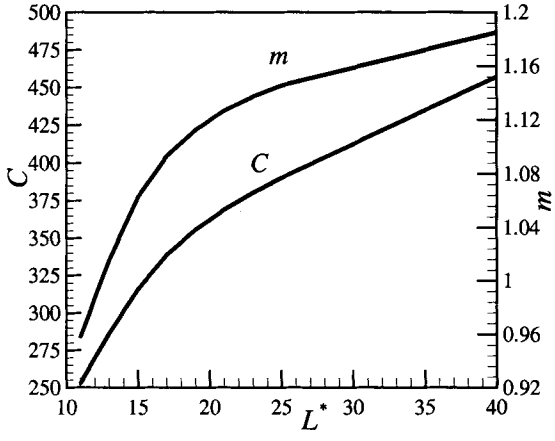

Fig.9 Correlation constant (C) and exponent (m) as a function of L^*

$$m = -0.0011(\lambda/a)^2 + 0.0529(\lambda/a) + 0.5216 \tag{13}$$

$$C = 0.016(\lambda/a)^4 - 1.0136(\lambda/a)^3 + 22.21(\lambda/a)^2 - 182.61(\lambda/a) + 685.27 \tag{14}$$

The above equations are valid for $11.0 \le L^* \le 40.0$, $100 \le Re \le 2000$, $3.5 \le D/a \le 12.8$ and show good agreement with calculated data within ±6% accuracy.

Heat transfer

Heat transfer rate is measured by local (Nu_x) and average (Nu_{av}) Nusselt numbers. Local Nusselt number distribution shows rise and fall in each cycle (Fig.10) and this tendency decreases with the increase of axial distance and wave number (n). Heat transfer rate is higher at converging parts and lower at the diverging parts of the pipe. Maximum heat transfer occurs near the reattachment point for each cycle. High velocity components normal to the wall occur[9] here, boundary layer is additionally reduced, leading to maximum heat transfer coefficient.

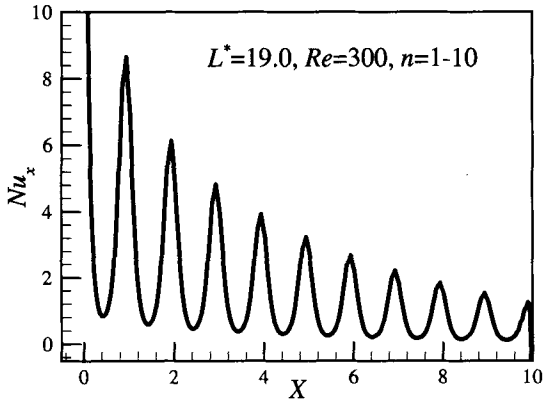

Fig.10 Local Nusselt number distribution for 10 cycle pipe showing exponential decay of Nu_x

Effect of surface waviness on heat transfer is shown in Fig.11. For higher waviness of the surface, Nusselt number shows lower value due to large recirculation bubble. Near the reattachment point heat transfer rate is higher for higher waviness of the surface. The physics behind this interesting scenario is well sighted from the Figs.12(a) and (b). Temperature gradient normal to the wall is lower inside the separation bubble (Fig.12(a)) for higher waviness of the surface compared to the same of the lower surface waviness (Fig.12(b)). Fig.13 shows the cycle average Nusselt number as a function of Reynolds number at different surface waviness where Nu_0 (=3.66) represents the Nusselt number for straight pipe at fully developed flow condition satisfying isothermal wall.

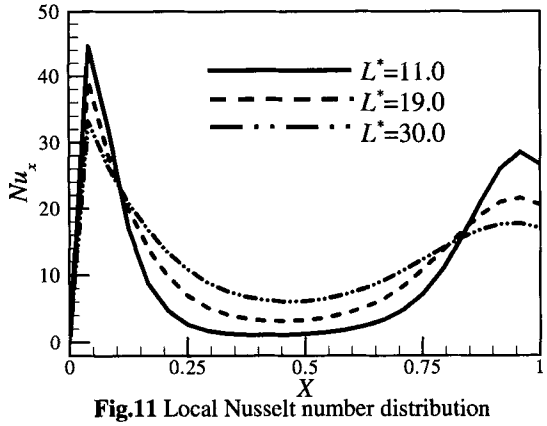

Fig.11 Local Nusselt number distribution

Conclusions

Present prediction gives an idea of flow field, pressure drop and heat transfer characteristics inside a sinusoidally varying wavy pipe. Higher the surface waviness earlier the flow separation, larger the pressure drop and higher the heat transfer rate. A correlation is

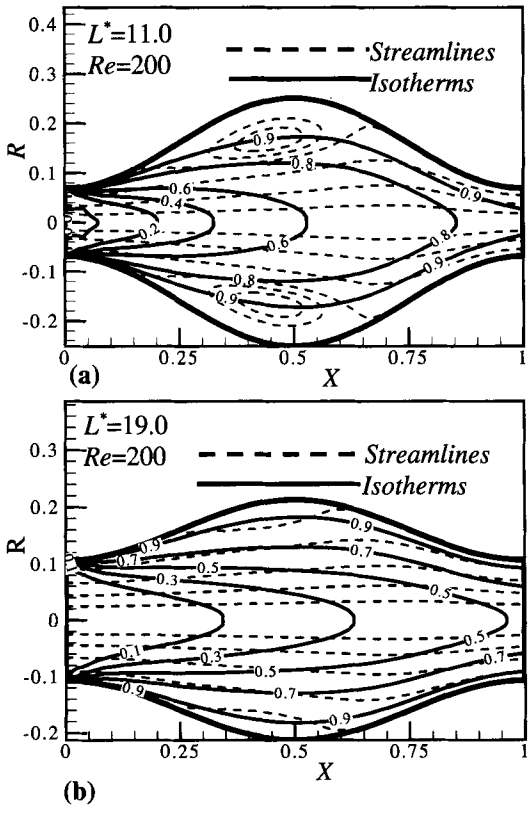

Fig.12 Combination of flow and thermal field

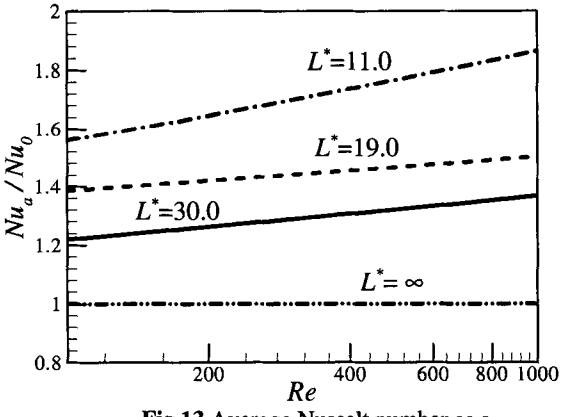

Fig.13 Average Nusselt number as a function of Reynolds number

proposed for calculating friction factor as a function of surface waviness and Reynolds number.

References

[1] C Saidi, F Legay, B Pruent Fotch. Laminar Flow Past a Sinusoidal Cavity. Int. J. Heat & Mass Transfer, 1987, 30(4)

[2] G Wang, S P Vanka. Convective Heat Transfer in Periodic Wavy Passages. Int. J. Heat & Mass Transfer, 1995, 38(17)

(*continued on page* 147)

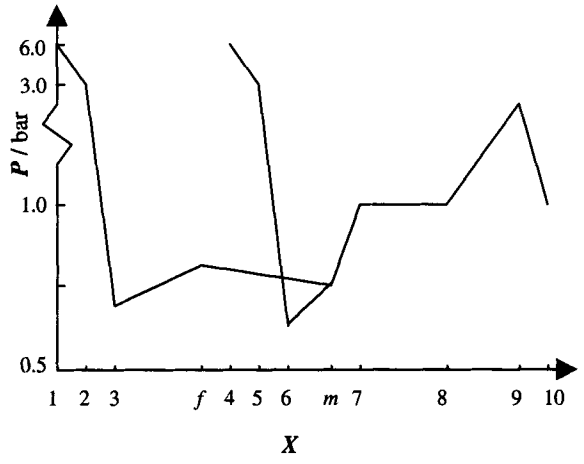

Fig.2 Variations in steam pressure on various cross sections of the flow system

Conclusions

1. Utilizing the principle of jet pressurization, the present expansion apparatus first gives rise to evaporation within the cells of the stuff, then causes the pressure of the stuff to be released suddenly, thus leading to an adequate expansion of the stuff.

2. When the ratio of the stuff mass rate of flow to the steam mass rate of flow is equal to 2.5, the pressurization ratio of the stuff is about 2.8 at the exit of the apparatus.

3. High levels of expansion are achieved indicating more than 75% relative increase in fill value of tobacco stem by means of the present expansion apparatus, and steam consumption per kilogram stem for the present expansion apparatus, which is required in the expansion process, is about 40% lower than that for conventional expansion apparatus.

References

[1] Pan, Fangsen. Explorations and Developmental Prospects on a New Type of Expansion Apparatus for Tobacco Stem, Tobacco Science & Technology, 1999, 3: 26-27

[2] Zhou, Moren. Fluid Mechanics, Pump and Blower, Chinese Construction Industry Press. 1979, 323 - 327

[3] Shen, Weidao et al.. Thermodynamics of Engineering, Higher Education Press. 1983, 50-52

(*continued from page* 138)

[3] C Yang, Y Asako, Y Yamaguchi, et al. Numerical Prediction of Transitional Characteristics of Flow & Heat Transfer in a Duct. Transaction of Heat Transfer, 1997, 119

[4] T Nishimura, Y Ohori, Y Kawamura. Flow Characteristics in a Channel with Symmetric Wavy Wall For Steady Flow. J. Chemical Engg. Japan, 1984, 466—471

[5] G Russ, H Beer. Heat Transfer & Flow Field in a Pipe With Sinusoidal Wavy Surface–Numerical Investigation. Int. J. Heat & Mass Transfer, 1997, 40(5)

[6] E M Sparrow, J W Comb. Effect of Interwall Spacing & Fluid Flow Inlet Conditions on a Corrugated-Wall Heat Exchanger. Transaction of ASME, 1983, 26(7)

[7] E M Sparrow, L M Hossfeld. Effect of Protruding Edges on Heat Transfer & Pressure Drop in Duct. Int. .J. Heat & Mass Transfer, 1984, 27(10)

[8] Y Asako, M Faghri, Finite Volume Solution for Laminar Flow & Heat Transfer in a Corrugated Duct. Transaction of ASME, 1987, 109

[9] G Russ, H Beer. Heat Transfer and Flow Field in a Pipe with Sinusoidal Wavy Surface –II Experimental Investigation. Int. J. Heat & Mass Transfer, 1997, 40(5)

[10] M Faghri, Y Asako. Numerical Determination of Heat Transfer & Pressure Drop Characteristic for a Converging-Diverging Flow Channel. Transaction of ASME, 1987, 109

[11] R S Amano. A Numerical Study of Laminar & Turbulent Heat Transfer in a Periodically Corrugated Wall Channel. ASME, 1985, 107

[12] J Ferziger, M Peric. Computational Methods for Fluid Dynamics. Springer Verlag, Berlin Heidelberg, 1996

[13] S V Patankar. Numerical Heat & Mass Transfer. McGraw-Hill Book Company, 1984

[14] S Mahmud. A Numerical Study of Heat Transfer & Fluid Flow in a Corrugated Channel. M. Sc. Engg. Thesis, Mech. Engg. Dept, BUET, Dhaka, 1999